SIAM J. Applied Dynamical Systems
Vol. 11, No. 3, pp. 939–962

Codimension-Two Homoclinic Bifurcations Underlying Spike Adding in the Hindmarsh–Rose Burster*

Daniele Linaro†, Alan Champneys‡, Mathieu Desroches§, and Marco Storace¶

Abstract. The Hindmarsh–Rose model of neural action potential is revisited from the point of view of global bifurcation analysis, with the singular perturbation parameter held fixed. Of particular concern is a parameter regime where lobe-shaped regions of irregular bursting undergo a transition to stripe-shaped regions of periodic bursting. The boundary of each stripe represents a fold bifurcation that causes a smooth spike adding transition where the number of spikes in each burst is increased by one. It is shown via numerical path-following that the lobe-to-stripe transition is organized by a sequence of codimension-one and -two homoclinic bifurcations. Specifically, each of a sequence of homoclinic bifurcation curves in the parameter plane is found to undergo a sharp turn, due to interaction between a two-dimensional unstable manifold and the one-dimensional slow manifold that persists from the singular limit. Local analysis using approximate Poincaré maps shows that each turning point induces an inclination-flip bifurcation that gives birth to the fold curve that organizes the spike adding transition. Implications of this mechanism for other excitable systems are discussed.

Key words. bifurcation analysis, codimension-two homoclinic degeneracies, Hindmarsh–Rose model, period adding

AMS subject classifications. 37C10, 37C29, 37M20, 37G15

DOI. 10.1137/110848931

1. Introduction.

The Hindmarsh–Rose (HR) model [19] is one of the most widely studied parameterized three-dimensional systems of ordinary differential equations (ODEs) that arises as a reduction of the conductance-based Hodgkin–Huxley model for neural spiking [20]. Its success comes from both its simplicity—there are just three ODEs with polynomial nonlinearity and only a few key parameters—and its ability to qualitatively capture the three main dynamical behaviors displayed by real neurons, namely, quiescence, tonic spiking, and bursting. Moreover, transitions between these behaviors can be easily described in terms of the biophysically motivated parameters. Even reduced-order models like the HR equations can have direct physiological meaning and so can be used to match or indeed predict detailed in vivo recordings; for instance, in [10] the authors use the HR model (after appropriately

*Received by the editors September 22, 2011; accepted for publication (in revised form) by E. Sander June 1, 2012; published electronically August 23, 2012.
http://www.siam.org/journals/siads/11-3/84893.html
†Biophysical and Electronic Engineering Department, University of Genoa, Genoa, Italy. Current address: Department of Biomedical Sciences, University of Antwerp, Belgium (daniele.linaro@ua.ac.be). The research of this author was partially supported by a Postdoctoral Fellowship of the Research Foundation - Flanders (FWO), under grant 12C9112N.
‡Department of Engineering Mathematics, University of Bristol, Bristol, UK (a.r.champneys@bristol.ac.uk).
§Department of Engineering Mathematics, University of Bristol, Bristol, UK. Current address: INRIA Paris-Rocquencourt Research Centre, BP 105, 781 Le Chesnay cedex, France (mathieu.desroches@inria.fr). The research of this author was supported by EPSRC under grant EP/E032249/1.
¶Biophysical and Electronic Engineering Department, University of Genoa, Genoa, Italy (marco.storace@unige.it).

rescaling the state variable x, the parameter I, and time) to fit the activity of both pyramidal cells and neocortical interneurons. Nevertheless, a key argument for their use is that they can point to generic understanding of which kinds of interventions or perturbations are likely to lead to certain kinds of transition. These understandings can then be used to help guide parameter searches for more in-depth computational models which can be investigated only by direct numerical simulation (DNS). In turn, these simulations can help guide experimental or clinical control strategies and protocols.

Many papers have investigated the bifurcations that occur in the HR model upon variation of one [4, 23, 41] or more [16, 39] of its parameters. These studies have typically focused on particular transitions—from periodic to irregular (chaotic) spiking-bursting dynamics, from tonic spiking to bursting, and on the two possible kinds of bursting (square-wave and pseudo-plateau). For perhaps the most comprehensive bifurcation analysis to date the reader is referred to the work of Shilnikov and Kolomiets [35].

In this paper we shall be concerned with understanding the complete bifurcation scenario that underlies the *smooth* transition from tonic spiking to bursting, paying particular attention to an observed sequence of spike adding transitions. This form of period adding behavior would cause a variation of the average number of spikes within a burst, and it is believed to have important physiological implications [31]. The key point of the paper is to show that codimension-one homoclinic bifurcations and their degeneracies are crucial to understanding how such transitions are organized in parameter space. The methodology we shall adopt will be a combination of brute-force methods, slow-fast arguments, numerical continuation (using AUTO-07P [14]), and geometric analysis using approximate Poincaré maps.

A key feature of the HR model is that it can be decomposed into a reduced two-dimensional "fast" ODE system with an additional slow variable. Such slow-fast arguments (see, e.g., [35] and references therein) can provide much generic information about the original model and tend to work best close to the singular limit of infinite time-scale separation. However, most physical systems operate away from the singular limit, and the mutual interactions between slow and fast dynamics are typically very subtle and give rise to further bifurcations in the complete system that occur in the singular limit.

Numerical continuation analysis [25] is typically quite robust, and, through its use of boundary-value problems to solve for recurrent trajectories, does not suffer from the same problems as DNS in the singular limit. Nevertheless, as we shall see, problems can still arise in the presence of "canard-like" phenomena [12, 17]. In this case, a mix of numerical results and geometrical analysis can prove pivotal, as is the case in this paper.

1.1. The Hindmarsh–Rose model. The phenomenological neuron model proposed by Hindmarsh and Rose [18, 19] is given by the following set of ODEs:

$$\begin{cases} \dot{x} = y - x^3 + bx^2 + I - z, \\ \dot{y} = 1 - 5x^2 - y, \\ \dot{z} = \mu \left(s \left(x - x_{rest} \right) - z \right). \end{cases} \tag{1.1}$$

The model is dimensionless, and the variables have only phenomenological interpretations. The variables x and y represent the fast charging dynamics (related to voltage and current,

respectively) associated with a single neuron, whereas z is a slow variable mirroring the action of slow ionic channels, which means that $0 < \mu \ll 1$. Hence, (1.1) is a slow-fast system with two fast variables and one slow variable. Its fast nullcline $M_{eq} := \{(x, y, z) \in \mathbb{R}^3;\ z = y - x^3 + bx^2 + I,\ y = 1 - 5x^2\}$ is the so-called *critical manifold* of the system. The critical manifold M_{eq} is a manifold of equilibria for the limiting problem obtained by setting $\mu = 0$ in (1.1) and called the *fast subsystem*. Furthermore, M_{eq} plays a crucial role in the nontrivial dynamics of the full system; see section 1.2 below. The roles played by the system parameters can be described as follows. The parameter I mimics the membrane input current for biological neurons, whereas b is an excitability parameter that allows one to switch between bursting and spiking behaviors and to control the spiking frequency. The parameter μ controls the time scale of the slow variable z, that is, the efficiency of the slow channels in exchanging ions. In the presence of spiking behavior, it affects the interspike interval, whereas in the case of bursting it affects the number of spikes per burst. The phenomenological parameter s governs the degree of adaptation in the neuron. A value of s around unity causes spiking behavior with no spike-frequency accommodation or subthreshold adaptation, whereas values around $s = 4$ (the value we shall use in this paper) allow strong accommodation and subthreshold overshoot and can even allow oscillations. The parameter x_{rest} sets the resting potential of the system and is usually set to -1.6 in the dimensionless units in which (1.1) is written.

Applying a slow-fast analysis to (1.1), the fast subsystem is given by the equations

$$\begin{cases} \dot{x} = y - x^3 + bx^2 + I - z, \\ \dot{y} = 1 - 5x^2 - y, \end{cases} \tag{1.2}$$

which contain only two out of the five initial parameters (b and I), but in the limit $\mu = 0$, z becomes a constant parameter.

In what follows, unless otherwise stated, we shall consider (1.1) at parameter values

$$s = 4, \qquad x_{rest} = -1.6, \qquad \mu = 0.01, \tag{1.3}$$

and we allow I and b to be bifurcation parameters.

1.2. Spike adding and slow-fast analysis. Typical spiking neurons occurring across biology can undergo a variety of distinct dynamical behaviors, according to the values of biophysical parameters. Among the most important behaviors, one may find [24] *quiescence*, which occurs when the input to the neuron is below a certain threshold and the output does not include any action potential firing events (or spikes); *spiking*, in which the output is made up of a regular series of spikes; *bursting*, where the output consists of groups of two or more spikes separated by periods of inactivity; and *irregular spiking*, where the output is made up of an aperiodic series of spikes.

Previous studies have shown that the HR model is able to reproduce all these dynamical behaviors; see [35, 39] and references therein. Specifically, one- and two-parameter bifurcation analysis has been used to unfold cascades of smooth transitions between stable bursting solutions and continuous spiking regimes, both regular (periodic) and irregular (chaotic). A key feature displayed by the HR model and many other neuronal models is the so-called spike adding mechanism. That is, by changing one parameter, it is possible to *sequentially* change the behavior of the system from spiking to bursting via transitions that add one spike to

each burst. In the HR model, changing the parameter b allows one to observe this transition among periodic responses. To some extent, also raising the injected current I leads to this spike adding, but this also typically increases the frequency of the bursts. Other combinations of parameters, e.g., μ and I, lead to similar results; see [16, 32, 39] and references therein.

In particular, the earlier paper [39] presented a comprehensive *brute-force* bifurcation diagram in the (b, I) parameter plane. The purpose of this paper is to explain a key feature of that work, namely, the nature of the global bifurcations that bound the region in which periodic spike adding is observed.

1.3. Outline. The rest of this paper is outlined as follows. Section 2 presents the numerical bifurcation analysis through numerical continuation. Particular attention is focused on an infinite family of bifurcation curves of homoclinic orbits that connect an equilibrium on the unstable part of the critical manifold to itself. Various codimension-two homoclinic bifurcation points are detected, and local bifurcation curves arising from them are computed. It is found that the key fold bifurcations underlying spike adding transitions originate from a sharp turning point along the homoclinic bifurcation curves, caused by the interaction between a one-dimensional slow manifold and a two-dimensional unstable manifold of an equilibrium point. Owing to the sharpness of the folding of the unstable manifold, numerical continuation is found to be inconclusive. Section 3 therefore presents a geometric analysis of such a situation and shows that there has to be an additional codimension-two homoclinic bifurcation of inclination-flip type very close to this point of interaction. An unfolding of the inclination flip gives the required extra curves of fold bifurcations. Finally, section 4 draws conclusions, suggests avenues for further work, and points to some wider implications of the results.

2. Numerical bifurcation results.

In particular, in this paper we will focus our attention on a specific portion in the (b, I)-plane brute-force bifurcation diagram obtained in [39]. One of the weaknesses of that method is that the presence of regions admitting coexisting asymptotic behaviors cannot be directly inferred from the color map, and the details of bifurcations can be smeared out in the process.

2.1. The regular-to-irregular bursting transition. In terms of bifurcation analysis, the area with the richest dynamics on the plane (b, I) occurs in the region $b \in [2.5, 3.2]$, $I \in [2, 4.5]$. Here we can observe lobe-shaped regions of irregular bursting and stripe-shaped regions of regular bursting, with each successive stripe corresponding to one extra spike per period. To try to understand the mechanism by which this transition from regular to irregular bursting regions occurs, Figure 1 shows a zoom of the parameter region in question with three different sets of bifurcation curves superimposed. These curves were computed using numerical continuation in the software AUTO-07P [14] and its extension HomCont for the localization of codimension-two homoclinic bifurcation points.

In the diagram, we have adopted the following color and labeling codes for the bifurcation curves:

- folds of cycles (tangent bifurcations) are labeled t and colored blue;
- period doublings (flips) are labeled f and colored red;
- homoclinic bifurcations are labeled h and colored black.

Moreover, a single superscript index indicates the approximate number of spikes per period

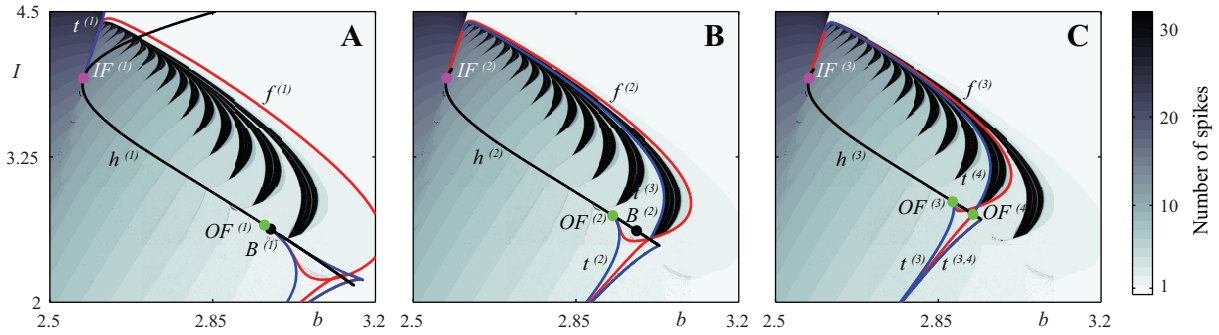

Figure 1. *Numerically computed bifurcation curves showing (in panels* A, B, *and* C, *respectively) bifurcations associated with one, two, and three bursts per period. See text for details.*

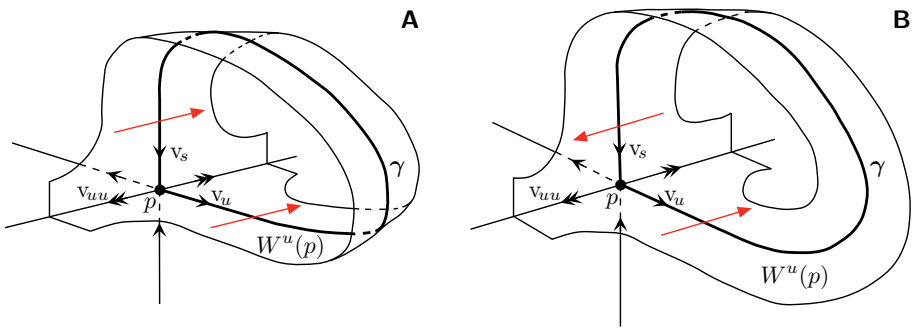

Figure 2. *Schematic representation of an inclination flip bifurcation in the case (relevant to* (1.1)*) of a saddle equilibrium in a three-dimensional vector field with a two-dimensional unstable manifold. The two panels show the same homoclinic orbit before (panel* A*) and after (panel* B*) the bifurcation; note how the unstable manifold changes from orientable to nonorientable between panels* A *and* B*, respectively. The notation is as described in section* 3 *below.*

of the limit cycle (or homoclinic orbit) undergoing the bifurcation. So, for example, the label $f^{(1)}$ indicates a period doubling bifurcation curve involving a 1-spike cycle. Note that each of the flips typically represents the first in an entire period doubling cascade. Superscripts (n, m) indicate that the cycle involved in the bifurcation undergoes a transition from n to m spikes, as is typical of bifurcations involved in the period adding mechanism. In addition, we use letters to distinguish distinct bifurcations of the same kind; e.g., $h^{(2)}$ and $h^{(2a)}$ will represent different homoclinic orbits that have two spikes.

In Figure 1 we have also identified several codimension-two homoclinic bifurcation points. Specifically purple, green, and black dots indicate, respectively, *inclination flip*, *orbit flip*, and *Belyakov* points. An inclination-flip bifurcation represents a point along a curve of homoclinic orbits to a real saddle at which the orientability of the global stable or unstable manifold changes; see Figure 2. For information on the complex codimension-one curves that can emanate from the codimension-two point, see, for example, [21, 22] and references therein. In particular, there are three topologically distinct cases. An orbit flip occurs when the trajectory undergoing the homoclinic orbit flips between the two components of the (weak) stable or unstable manifold. In the case of a real saddle in three dimensions, the same three

topological cases apply as for the inclination flip; again see [33, 21] and references therein. A Belyakov bifurcation [1, 2, 3] occurs when the leading eigenvalues (closest to the imaginary axis) of the saddle-point involved in the homoclinic orbit are double and undergo a transition to a complex pair. More precisely, there are three kinds of Belyakov codimension-two points: transition from saddle to saddle-focus with a saddle index less than 1, saddle-focus with saddle index equal to 1, and what is called a Shilnikov–Hopf bifurcation.

The theory predicts the presence of several families (of infinite cardinality) of bifurcation curves originating at these points and accumulating exponentially on the homoclinic curve. See [6, 26, 38] for more details of the dynamics near codimension-two homoclinic bifurcations.

As we shall see in more detail shortly, these codimension-two points, and more besides, play a key role in unfolding the regular-to-irregular bursting transitions.

Note that each of the three homoclinic bifurcation curves computed in Figure 1 actually represents an approximate double cover of the same curve in parameter space, with the seeming endpoint of the curve in fact representing a sharp U-turn. Therefore, the fine structure of the bifurcation curves is not apparent without looking at the particular shapes of the trajectories, which will be elucidated in the following subsections and also through sketches. The structure of the homoclinic curve $h^{(3)}$ and the associated local bifurcations of cycles depicted in panel C of Figure 1 is similar to that relevant for all subsequent lobe-to-stripe transitions for $k > 3$. Therefore, the case $k = 3$ will serve as an illustrative example in what follows. The cases for $k = 1$ and $k = 2$ (depicted in panels A and B, respectively) are special and will be dealt with separately.

Before proceeding with a more in-depth examination of the homoclinic bifurcations, it is worth showing how the local bifurcations of cycles that bifurcate *below* (for lower I-values) the homoclinic bifurcation curves organize the boundaries of the stripe-shaped periodic bursting regions. Figure 3 shows in detail the bifurcations associated with the spike adding boundary between the 3-spike and 4-spike regular bursting regions. Note that the transition is hysteretic; that is, there is a parameter window of bistability in which both 3- and 4-spike regular bursting can be observed.

Panel A of the figure shows the nature of the transition under variation of b. Upon decreasing the parameter from the point labeled S, the stable 3-spike cycle (labeled a) becomes unstable through a fold $t^{(3)}$, leading to interval of unstable 3-spike cycles (such as the one labeled b), until another fold $t^{(3,4)}$, after which it remains unstable. The branch then restabilizes at a period doubling bifurcation $f^{(4)}$ to form the 4-spike cycle labeled c. Upon further decrease of b, this stable 4-spike cycle will remain until a further bifurcation $t^{(4)}$ (not shown in this sketch), and the whole process repeats for the 4-to-5-spike cycle transition. Thus from the point of view of a single limit cycle, the whole spike adding process from one to many can be thought of as a single *smooth* process.

Panel B of Figure 3 shows a zoom from Figure 1C of the bifurcation curves that are involved in the spike adding mechanism. Note, in particular, that two of the crucial codimension-one bifurcations involved, $t^{(3)}$ and $f^{(4)}$, originate in the parameter plane from two distinct orbit flips that lie on the apparent $h^{(3)}$ homoclinic bifurcation curve. The other local bifurcation curves involved, $t^{(3,4)}$ and $f^{(3,4)}$, appear to originate from the endpoint of the homoclinic curve. As we shall show in section 3, these bifurcation curves are actually caused by an inclination flip that occurs at this apparent endpoint.

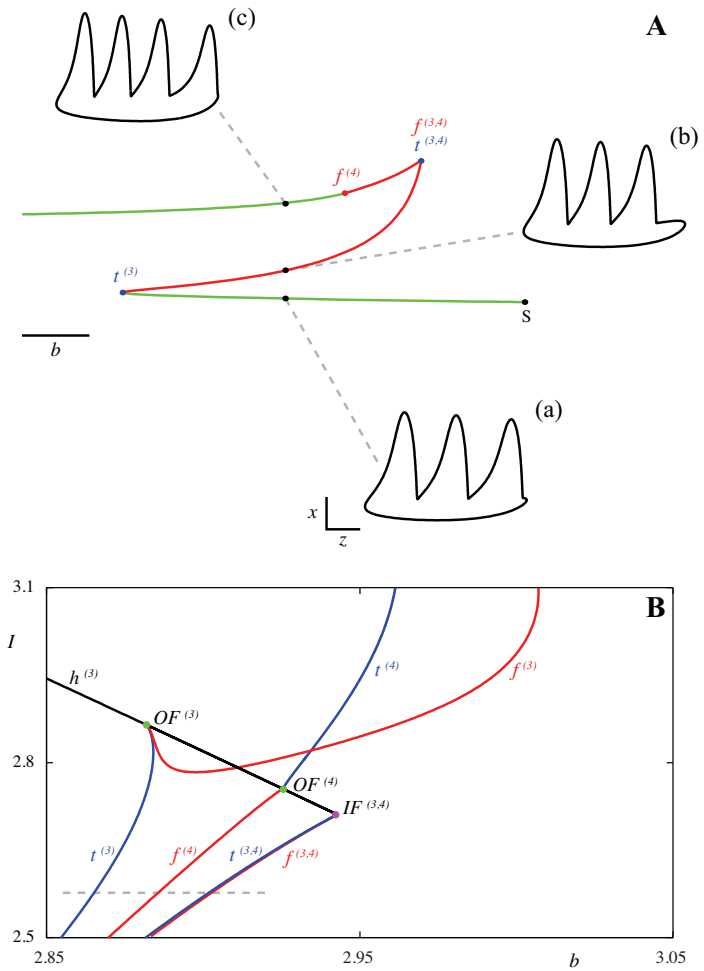

Figure 3. *Sketch of the period adding mechanism and corresponding bifurcation curves. In panel* A *the colored traces indicate the maximum z coordinate of the solution; color encodes stability: Green is stable, and red is unstable. The trajectories a, b, and c are projections on the (z,x)-plane of the full three-dimensional solution. Panel* B *shows the actual orbit flip points and the bifurcation curves that take part in the period adding mechanism. The continuation shown in panel* A *can be obtained by following, for example, the dashed grey line that crosses $t^{(3)}$, $f^{(4)}$, $t^{(3,4)}$, and $f^{(3,4)}$.*

2.2. The homoclinic curve $h^{(1)}$. The first characteristic feature of each homoclinic curve $h^{(k)}$ is its U-shape, as qualitatively sketched in Figure 6 for the lower part of the homoclinic curve $h^{(3)}$ (this curve is depicted only qualitatively). In fact, the U-turn is so sharp that it can be detected only on a very small scale in the parameter space, and on any wider scale, as in Figure 1A, the two branches appear almost as a double cover of the same curve. Note that, as the U is traced, there is a transition between a homoclinic with k spikes and one with $k+1$ spikes. Such sharp U-turns of homoclinic orbits have been observed in other systems (see, e.g., [27, 9]) and are typically characterized by orbits gaining an extra spike or pulse.

The homoclinic bifurcation curve $h^{(1)}$ is reported (panel A) and sketched (panel B) in Figure 4. In this and subsequent similar figures bifurcation curves are both shown as they

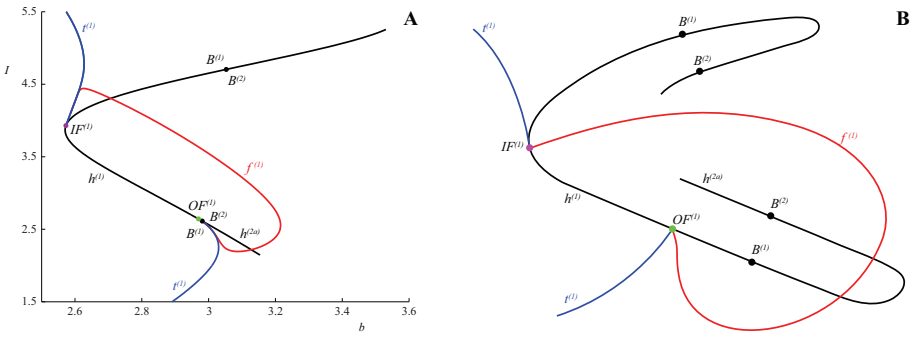

Figure 4. *Real (panel* A*) and sketched (panel* B*) bifurcation structure around* $h^{(1)}$*: Note the presence of just one flip bifurcation* ($f^{(1)}$) *that connects the inclination flip point* $IF^{(1)}$ *to the orbit flip point* $OF^{(1)}$.

really are (numerically detected by AUTO-07P) and depicted in an exaggerated way in a pseudoparameter plane in order to elucidate their topological features. The key feature here is an inclination-flip point labeled $IF^{(1)}$ that separates two portions of the homoclinic branch that are both U-shaped. We shall focus on the lower portion. The inclination flip in this case is of type B according to the classification reported in [21] and [30, Fig. 7]; there are single curves of period doubling and a fold of cycle bifurcations emanating from the codimension-two point. Following the branch $h^{(1)}$ away from the inclination flip, we find an orbit flip. Again, two other curves of local bifurcations emanate—a period doubling and a fold. Note how the period doubling bifurcation $f^{(1)}$ connects the two codimension-two points $IF^{(1)}$ and $OF^{(1)}$, whereas the two folds of cycle curves labeled $t^{(1)}$ are distinct. We also note the presence of Belyakov points, labeled as $B^{(1)}$ on the 1-spike branch $h^{(1)}$ and as $B^{(2)}$ on the 2-spike branch $h^{(2a)}$. Between these two points along the homoclinic curve, the saddle equilibrium is actually a saddle focus (with complex eigenvalues). With respect to this figure, in Figure 1 (panel A) one further period doubling and two folds of cycle (meeting at a cusp point) curves are displayed (right bottom corner). One of these folds of cycles is rooted at the Belyakov point $B^{(1)}$.

The numerical continuation suffers convergence problems along the branches of 2-spike homoclinic orbits as they return toward $IF^{(1)}$ and are depicted to end in "mid air." The eventual fate of the multispike branches remains an open issue which we shall not address here, partly because they do not seem to play any further role in the regular-to-irregular bursting transition of interest in this paper.

2.3. The homoclinic bifurcation curves $h^{(k)}$ and their degeneracies. The qualitative feature of the homoclinic bifurcation curve $h^{(3)}$, which is sketched in Figure 5, is valid for any $k \geq 3$. The fundamental difference with respect to $h^{(1)}$ is the absence of any Belyakov point. This is due to the fact that the whole homoclinic curve lies in a region of the parameter plane where the eigenvalues of the equilibrium involved in the homoclinic trajectory are real. The curve $h^{(3)}$ emanates from an inclination-flip point $IF^{(3)}$, which appears to be distinct from $IF^{(1)}$ but occurs nearby in parameter space. One distinction from the previous case is that the inclination flip is now of type C, which means that an entire period doubling cascade emanates, as do multiple-pulse homoclinic orbits for all periods ($h^{(3)}$, $h^{(6)}$, ...). These

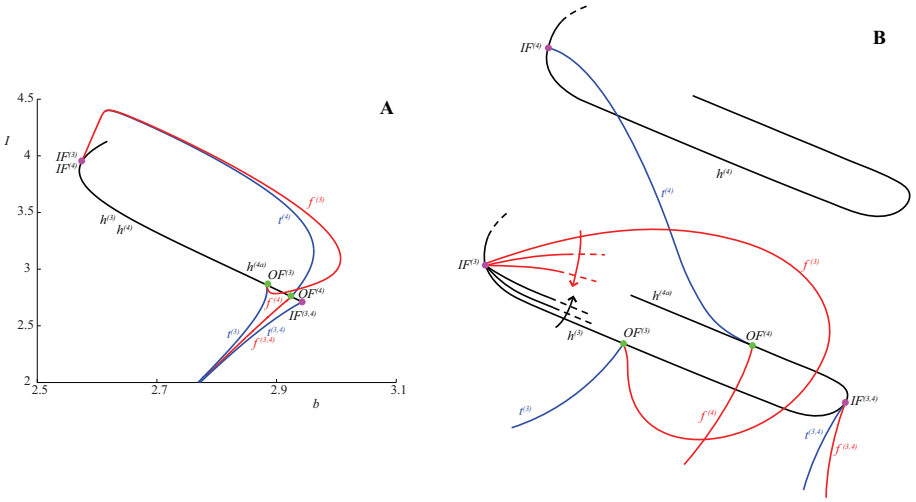

Figure 5. *Real (panel* A*) and sketched (panel* B*) bifurcation structure around the kth homoclinic bifurcation* $h^{(k)}$*. In this particular sketch,* $k = 3$*, but the general sketch is valid for any* $k \geq 3$*. For completeness, the sketch also shows the homoclinic curve for* $k = 4$*. This undergoes the same sequence of bifurcations as* $h^{(3)}$*, which are not depicted.*

cascades are illustrated schematically via the sequence of lines superimposed with curved arrows in Figure 5. We do not focus here on these additional bifurcations. Also, there are again computational difficulties with determining precisely what happens to the branch on the "far" side of $IF^{(3)}$, or to the homoclinic curve $h^{(4a)}$ as it returns toward the vicinity of $IF^{(3)}$. Instead we focus on the transitions that occur close to the U-turn as $h^{(3)}$ transitions into $h^{(4a)}$.

Each branch of the U-turn undergoes two orbit-flip bifurcations:

- $OF^{(3)}$, where the first bifurcation of the period doubling cascade ends and meets a fold of cycles (respectively, $f^{(3)}$ and $t^{(3)}$ in Figure 5).
- $OF^{(4)}$, where $t^{(4)}$ and $f^{(4)}$ are rooted: the former is connected with $IF^{(4)}$ on the primary homoclinic bifurcation of the subsequent homoclinic doubling cascade, whereas the latter takes part in the period adding process, as described in Figure 3.

Very close to the tip of the U-shaped homoclinic bifurcation, there is an additional inclination-flip point, labeled $IF^{(3,4)}$ in Figure 5. From this point, the two curves $t^{(3,4)}$ and $f^{(3,4)}$ are born, which are the additional bifurcations that take part in the spike adding process depicted in Figure 3. However, we have not been able to numerically detect $IF^{(3,4)}$, due it would seem to the very sharp turn of the homoclinic curve, but we can infer its presence as we now explain. Furthermore, the geometric analysis in section 3 shall provide more careful justification for the presence of this bifurcation.

Figure 6 shows more details of the orbits close to the U-turn, which provides further evidence for the presence of the additional inclination flip $IF^{(3,4)}$. In this figure, the central U-shaped curve represents the homoclinic bifurcation, and the eight surrounding panels display the homoclinic trajectories (black thick lines) at significant points on the curve, superimposed onto the bifurcation diagram of the fast subsystem (thin colored lines and points).

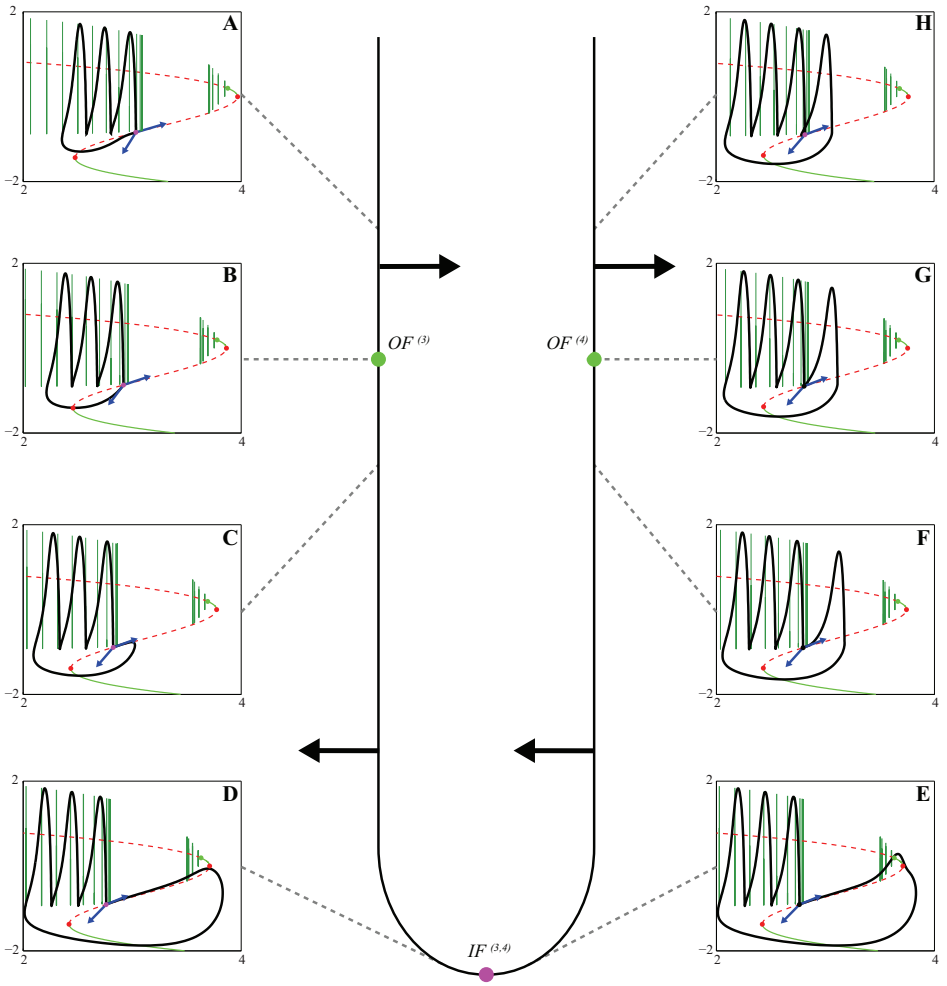

Figure 6. *Representation of how the homoclinic trajectories change along the U-shaped homoclinic bifurcation curve $h^{(3)}$. Each panel contains the homoclinic orbit (thick black line) on the plane (z, x) and the results of a bifurcation analysis of the slow-fast subsystem of (1.2) (thin colored lines and dots); the blue arrows are the unstable eigenvectors of the saddle node equilibrium. The arrows in the central panel, on the parameter plane, indicate the direction of bifurcation of periodic orbits from the homoclinic bifurcation curve. For a detailed description of each panel, see the main text.*

In particular, there is the manifold of equilibria M_{eq}, represented by a solid green (stable) line and a dashed red (unstable) line, which undergoes two folds (red dots) and a supercritical Hopf bifurcation (green dot); the grey vertical lines are the projections onto the (z, x)-plane of the stable limit cycles of system (1.2), which organize the *bursting* behavior of the full HR model; the periodic solutions of the fast system do not constitute a unique "funnel," but rather they are separated into two distinct sets, due to the presence of two homoclinic bifurcations in the fast subsystem, at the coordinates where the periodic solutions accumulate.

Panels A and H of Figure 6 are "above" $OF^{(3)}$ and $OF^{(4)}$, respectively, on opposite branches of the homoclinic curve: in both panels, the homoclinic trajectory leaves the saddle

node along the leading unstable direction and returns along the only stable direction after three (panel A) or four (panel H) turns. Panels B and G correspond to the orbit-flip points $OF^{(3)}$ and $OF^{(4)}$, respectively: it can be clearly seen how the homoclinic trajectory leaves the saddle node along the nonleading unstable direction. Again, the trajectory returns to the equilibrium point after three (panel B) or four (panel G) spikes. Panels C–F are located between $OF^{(3)}$ and $OF^{(4)}$, and their purpose is to illustrate the qualitative changes that the homoclinic trajectory undergoes between the two orbit-flip points and especially near the tip of the homoclinic curve, where we conjecture the presence of the inclination-flip point $IF^{(3,4)}$. In particular, in panels C and E it can be observed how the homoclinic trajectory leaves the saddle node again along the leading unstable direction, but this time in the opposite sense than in panels A and H. This makes the homoclinic orbits sort of *canard cycles* that spend a large amount of time on the *unstable* part of the slow manifold. In the $0 < \mu \ll 1$-regime of the HR model it has been shown that canard trajectories (not specifically homoclinic orbits) of this kind exist for a wide range of parameters, and they are known to be directly involved in the spike adding mechanism [11, 17, 40]. Finally, panels D and E are topologically similar to panels C and F, with the only difference being that, being so close to the tip of the homoclinic curve, the canard orbits are *maximal*: in particular, when the orbit goes past the upper fold of equilibria in the fast subsystem, an additional turn is added to the trajectory, which is the fundamental mechanism behind period adding in this and other models. Numerical evidence shows that this happens exactly at the parameter values corresponding to the tip of the homoclinic bifurcation curve.

The arrows in the central panel of Figure 6 indicate the direction of bifurcation of periodic orbits from the homoclinic bifurcation curve: the three points $OF^{(3)}$, $OF^{(4)}$, and $IF^{(3,4)}$ divide the homoclinic curve into four distinct regions. By going from one region to the other, the direction of bifurcation of periodic orbits changes, due to the presence of the orbit-flip degeneracies and of the turning point at the tip of the U-shaped curve: this gives a first, intuitive, indication that another degeneracy point where the homoclinic bifurcation undergoes side-switching must be present. There are three such generic codimension-two points that lead to side-switching in the case that the saddle point is a real saddle; these are orbit flip, inclination flip, and resonant eigenvalues. The latter occurs when $\mu_1 = -\lambda_1$, where μ_1 is the stable eigenvalue of the saddle point and λ_1 is the weakest unstable eigenvalue. We can easily check that the eigenvalue condition is not satisfied, and we can rule out the presence of an orbit flip, since the direction along which the trajectory leaves the saddle node does not change. Hence we are left only with the possibility that the point at the tip is indeed an inclination flip. A very similar structure has been found in [5, Fig. 19] in another context. However, in section 3 we shall prove categorically that an inclination flip occurs very close to the sharp turning point.

We finally remark that Shilnikov [36, 37] proved and pointed out the conditions, originally called the change of the leading direction and the sign change of the separatrix value (actually more meaningful compared to orbit and inclination switches), under which the homoclinic loop bifurcation of a hyperbolic saddle results in a single saddle periodic orbit.

2.4. The special case $k = 2$. The homoclinic bifurcation curve $h^{(2)}$ is sketched in Figure 7 (the real curves were superimposed on the brute-force bifurcation diagram in panel B

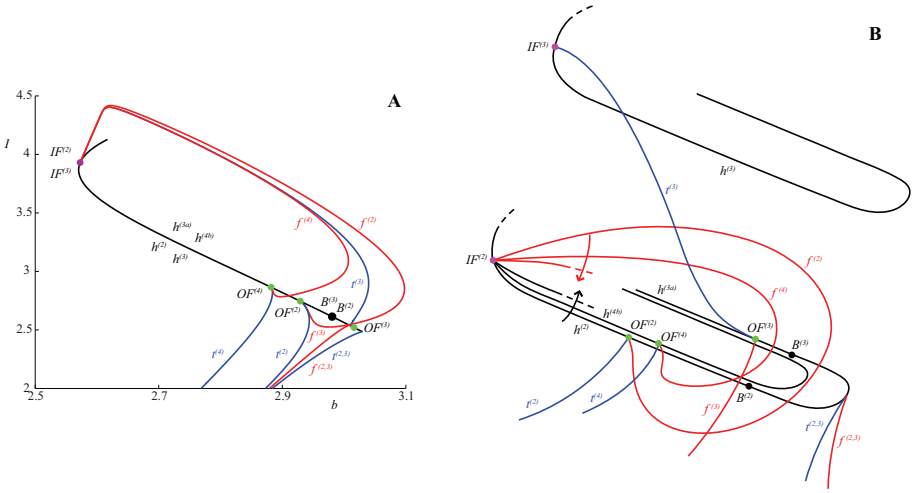

Figure 7. *Real (panel* A*) and sketched (panel* B*) bifurcation structure around* $h^{(2)}$*: The inclination flip point* $IF^{(2)}$ *gives birth to both a homoclinic doubling and a period doubling cascade. Note the presence of two Belyakov points,* $B^{(1)}$ *and* $B^{(2)}$*.*

of Figure 1). Here we also compute a separate homoclinic curve $h^{(4b)}$ with four spikes that also comes out of the inclination flip point $IF^{(2)}$, which again appears to be distinct from $IF^{(1)}$ although nearby it in parameter space. This curve exists because the inclination flip is of type C and is the first in an infinite sequence of the subsidiary homoclinic bifurcations that emanate from the codimension-two point. Like in the general case for $k > 2$, each homoclinic branch emanating from the IF has an orbit flip. The fold bifurcation $t^{(2)}$ is the one that is directly involved in the spike adding from two to three spikes similarly to what shown in Figure 3 for the 3-to-4-spikes transition. A connection between the homoclinic curves $h^{(3a)}$ and $h^{(3)}$ is provided by the fold of cycles $t^{(3)}$: this latter bifurcation terminates the chaotic region that is born with the period doubling cascade that starts with $f^{(2)}$, as can be seen in panel A.

The curves $t^{(2,3)}$ and $f^{(2,3)}$ converge on the tip of the U-turn. Note that there can be no inclination flip in this case, because between the two Belyakov points $B^{(2)}$ and $B^{(3)}$ the equilibrium has complex eigenvalues.

3. Analysis of inclination flip due to fold in slow manifold. The purpose of this section is to show theoretically the presence of an inclination-flip codimension-two point at the sharp turning points of each of the curves $h^{(k)}$ with $k > 2$. Moreover, we aim to show that this process is a natural consequence of the sharp folding in the curve of homoclinic orbits and that this sharp turn is itself a consequence of the canard-related transition of an n-spike homoclinic orbit into an $(n + 1)$-spike homoclinic orbit. Furthermore, by constructing an approximate return map around the critical homoclinic orbit, we are able to derive asymptotic expressions for the curve of the saddle node of limit cycle bifurcations that emanates from this codimension-two point.

The method of analysis is the standard one (see, e.g., [38]) of constructing the return map as a composition of approximate Poincaré maps in a full neighborhood of both parameter and

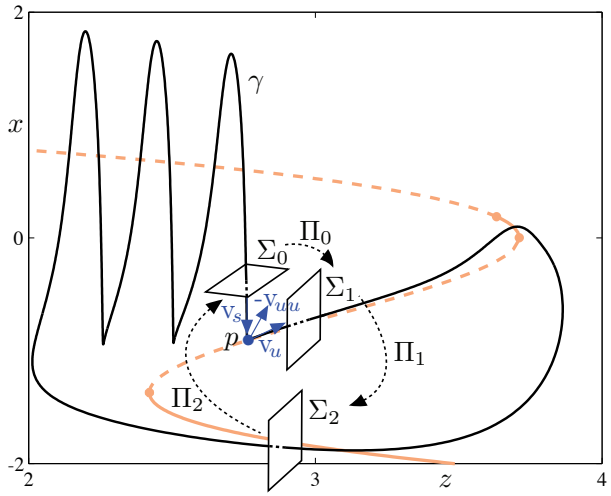

Figure 8. *A 3-spike homoclinic orbit γ of system (1.1) projected onto the (z,x)-plane and superimposed onto the bifurcation diagram of the fast subsystem. The values of parameters b and I for this orbit correspond to the tip of the homoclinic curve computed in [28] and, hence, to the conjectured inclination-flip bifurcation. We also show the saddle equilibrium p together with its strong unstable, weak unstable, and stable eigendirections v_{uu}, v_u, and v_s, respectively. The three cross-sections Σ_i, $i = 0,\ldots,2$, allow us to construct a return map Π from Σ_1 back to itself, in order to study the behavior of nearby trajectories (for fixed b and I close to the transition of interest).*

phase space of the codimension-two point in question; see Figure 8. The analysis is general and can apply to any three-dimensional system with the same generic features as the HR model. However, the key hypothesis has to be justified numerically (in subsection 3.1); this is namely that the forward image of any smoothly parameterized set of trajectories that interacts transversely with the fold of the critical manifold of the slow-fast system undergoes a sharp fold when viewed in any transverse Poincaré section. This assumption is formalized in the construction of the map Π_2 in subsection 3.2 below.

3.1. The process of spike adding. It is useful to examine in detail what happens to the trajectory of the homoclinic orbit as it passes close to the sharp turning point in one of the loops of the loci of homoclinic orbits. Consider Figure 8, which depicts just such an orbit that is undergoing a transition from three to four spikes at parameter values $b = 2.9427488761$, $I = 2.7111448924$. We shall henceforth refer to these as the critical parameter values. Note that the nascent fourth spike forms via the interaction of the unstable manifold with the fold point of the critical manifold (depicted by a dashed red line). Figure 6 shows homoclinic orbits on the branch just before (panel D) and just after (panel E) this critical codimension-two orbit.

Figures 9 and 10 show the results of a numerical computation of a portion of the unstable manifold of the saddle point at the critical parameter values. The map shown in Figure 9 (panel B) was computed by variation of a transverse coordinate in the unstable manifold close to the equilibrium point p and computing until the first return to a Poincaré section given by $z = 2.75$. In particular, the set U_1 of initial conditions chosen was of the form

$$U_1 = \{(x,y,z) = p + \varepsilon \mathrm{v}_u + \theta \mathrm{v}_{uu} | \text{ for } \theta \in (-\varepsilon,\varepsilon)\},$$

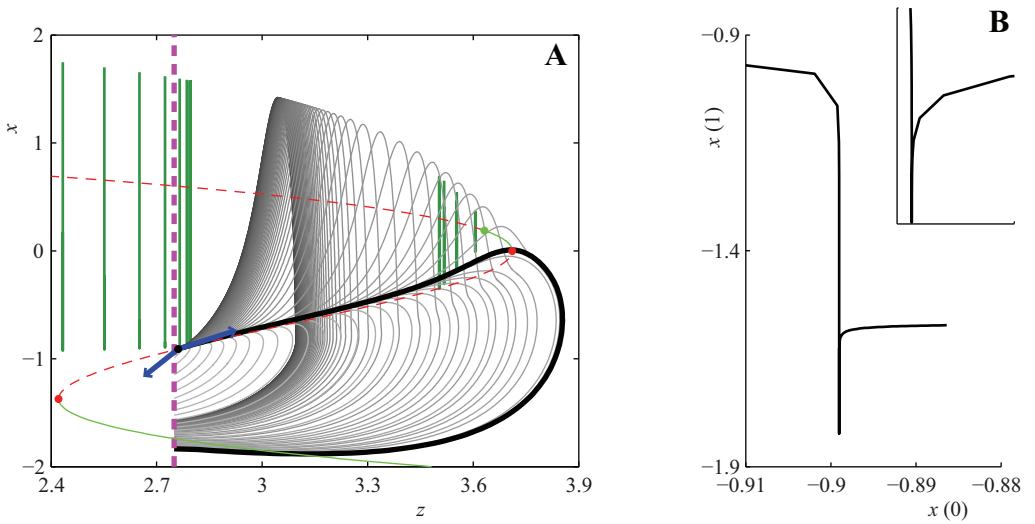

Figure 9. *(Panel* A*) Trajectories in the unstable manifold at the critical parameter values* $b = 2.9427488761$, $I = 2.7111448924$. *(Panel* B*) Approximate one-dimensional map showing that the unstable manifold of the homoclinic trajectory is folded. For a detailed description of each panel, see the main text.*

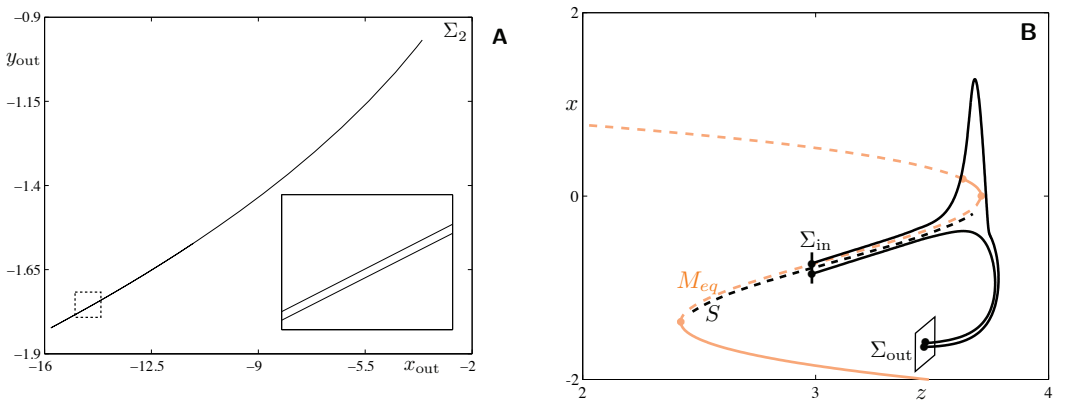

Figure 10. *(Panel* A*) Image of the initial conditions* U_1 *computed as in Figure* 9 *projected onto the* x *and* y *coordinates of the outgoing Poincaré section* $z = 2.75$. *(Panel* B*) Schematic representation of a general slow-fast system in three dimensions with a saddle-type slow (Fenichel) manifold* S *and an underlying critical manifold* M_{eq} *that is folded. Also shown are two orbit segments with very close initial conditions; only one gets a twist when passing close to the upper fold of* M_{eq}*, due to the relative position of its initial conditions with respect to* S.

where $\varepsilon = 0.1$ was chosen to give a close approximation to the unstable manifold $W^u_{\rm loc}(p)$ in a neighborhood of the critical homoclinic orbit. Since the unstable manifold is an invariant set, the theory predicts that trajectories that start on the manifold should remain on it indefinitely: unfortunately, due to errors in the numerical integration of this slow-fast system close to the critical manifold, such a result cannot be obtained with standard integration techniques. However, it is possible to overcome this problem by resorting to *continuation* techniques by

setting up a proper boundary-value problem (BVP), where one of the parameters that are allowed to vary is the integration time. This particular technique has been exploited, for example, in [13] to compute part of the manifold of the Lorenz equations.

By solving BVP with AUTO-07P, we can obtain the results shown in Figure 9. As in previous figures, in panel A the thin colored lines represent the bifurcation diagram of the fast subsystem, and the blue arrows are the unstable eigenvectors of the saddle node equilibrium. The purple dashed line is the section that constitutes the terminating point of the integrations. The thin grey lines are the integrations of the system obtained by varying the parameter θ in the range $[-0.1, 0.1]$; the thick black line is a piece of the homoclinic trajectory that satisfies the boundary conditions and is used to start the continuation procedure (which corresponds to $\theta \approx -0.001$). Panel B shows an approximate one-dimensional map of the initial versus the final x-coordinate. It can be clearly seen that such an approximate map is not invertible (see also the inset, which contains a zoom of the central part); i.e., two distinct initial conditions lead to the same final condition. This constitutes a further justification of our conjecture, since it shows that the unstable manifold of the homoclinic trajectory is folded.

To show this folded manifold in more detail, we depict in Figure 10 (panel A) the image of U_1 in the Poincaré section $z = 2.75$. Note the folded shape of the image of U_1. We conjecture that this fold is a direct consequence of a portion of the unstable manifold passing close to the fold point of the critical manifold M_{eq}. This conjecture is confirmed by noting from the computation of the trajectories in question in Figure 9 that the region of the sharp turning point in the image of U_1 corresponds to the trajectories that pass the closest to the fold in M_{eq} (actually since Figure 9 was computed at the critical parameter values, the trajectory that corresponds to the closest point to the fold is on the homoclinic orbit). A similar passage near such a fold of the critical manifold has previously been found in the HR model and has previously been shown to underlie spike adding at the level of periodic orbits. It was first reported by Terman [40, 41], who focused on chaotic dynamics in between n-spike and $(n + 1)$-spike orbits as well as the disappearance of bursting upon parameter variation. This mechanism has been studied more recently using the framework of slow-fast dynamical systems in [17].

We show in Figure 10 (panel B) a schematic representation of the dynamical behavior suggested by our numerical results. We depict a three-dimensional slow-fast system with all the generic features of the HR model—two fast variables and, hence, a one-dimensional critical manifold M_{eq}. The figure shows the projection onto the (z, x)-plane, where z is slow and x is fast, and we superimpose two segments of trajectories with initial conditions chosen to be very close to one another and to M_{eq}. When M_{eq} is cubic-shaped (i.e., with two fold points) and when its middle branch is composed by saddle equilibria of the fast subsystem, then away from the fold points this middle branch perturbs smoothly with respect to the small parameter ε to a saddle slow (Fenichel) manifold S [15]. In this configuration, one can observe at the level of both transient and long-term dynamics nearby trajectories and attractors that diverge from one another when one gains an extra twist as it passes close to the upper fold of M_{eq}, whereas the other does not; see two such orbit segments in Figure 10. This particular dynamical behavior can be understood by further looking at the underlying slow-fast structure of the problem. Indeed, the families of (un)stable manifolds $W^{u,s}(p)$ of the saddle equilibria p associated with the fast dynamics perturb smoothly to stable and unstable

manifolds $W^{u,s}(S)$ of the Fenichel manifold S [15]. Then, if initial conditions are taken close to but on opposite sides of the unstable manifold of S, they will follow S for some time until one trajectory jumps up and the other continues down. The trajectories that jump up cause an extra twist in that portion of the manifold.

Thus, these numerical results provide strong justification that the process of spike adding is caused by the portion of the trajectory of the homoclinic orbit that is closest in time to the local unstable manifold passing close to the fold point of the slow manifold. In turn, such a passage causes a sharp fold in the forward image of the local unstable manifold. The aim of the rest of this section is then to argue that this process causes a sharp turning point in parameter space of the locus of homoclinic orbits and that there is necessarily an inclination-flip bifurcation point there. Moreover, a fold curve of periodic orbits and a period doubling bifurcation curve emanate from the inclination flip.

3.2. Construction of Poincaré return map. Consider a sufficiently smooth three-dimensional vector field

$$\dot{x} = f(x, \mu), \qquad x \in \mathbb{R}^3, \quad \mu \in \mathbb{R}^2,$$

that has a saddle point p with real eigenvalues $\lambda_{uu} > \lambda_u > 0 > \lambda_s$, with corresponding eigenvectors v_{uu}, v_u, and v_s. We assume for simplicity (after a parameter dependent change of coordinates if necessary) that the location of and linearization at p is parameter independent. Suppose that, at a critical codimension-two point $\mu = 0$, a homoclinic orbit $\gamma(t)$ to p exists that satisfies certain nondegeneracy hypotheses:

(H1) $\gamma(t) \to p$ as $t \to \pm\infty$.

(H2) $\gamma(t)$ is tangent to v_u as $t \to -\infty$ and specifically approaches p along the positive v_u direction.

We also suppose that the sign of v_s has been chosen so that $\gamma(t)$ approaches p along the positive v_s direction as $t \to +\infty$.

(H3) The map Π_2 (defined below) is degenerate such that it can be described by the given quadratic form to leading order.

(H4) The parameter μ unfolds this codimension-two singularity in a generic way. (Specific choices for $\mu = (\mu_1, \mu_2)$ are defined below.)

We begin the analysis by considering three separate Poincaré sections Σ_0, Σ_1, and Σ_2 as depicted in Figure 8 for the HR model and in Figure 11 for a general system. The cross-sections Σ_0 and Σ_1 are defined in terms of local coordinates (ξ_1, ξ_2, ξ_3) corresponding to projection along the three-dimensional basis $(\mathrm{v}_s, \mathrm{v}_u, \mathrm{v}_{uu})$. Specifically, let

$$\Sigma_0 = \{(\xi_1, \xi_2, \xi_3) | \xi_1 = \varepsilon\}, \qquad \Sigma_1 = \{(\xi_1, \xi_2, \xi_3) | \xi_2 = \varepsilon\}$$

for $0 < \varepsilon \ll 1$.

The section Σ_2 is chosen to be transverse to the flow at a point $\gamma(0)$ along the critical homoclinic orbit, at an $O(1)$ distance from p. Let local coordinates (η_1, η_2) be chosen within Σ_2 such that $\gamma(0)$ is at the origin and the tangent vector to $W^u(p) \cup \Sigma_2$ at γ_0 lies along the η_1-axis. Furthermore, after a parameter dependent change of coordinates if necessary, we shall suppose that the flow from Σ_1 to Σ_2 is independent of the unfolding parameters μ. A convenient choice of unfolding parameters is to assume that the intersection between Σ_2 and

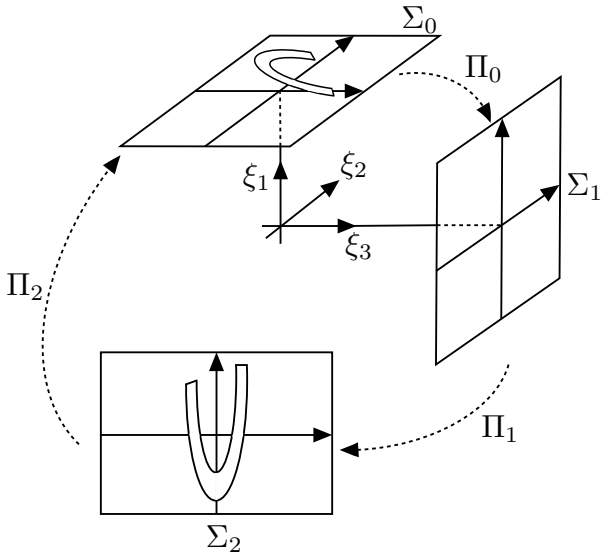

Figure 11. *Poincaré sections Σ_0, Σ_1, and Σ_2 for the study of the inclination-flip bifurcation in a general three-dimensional system.*

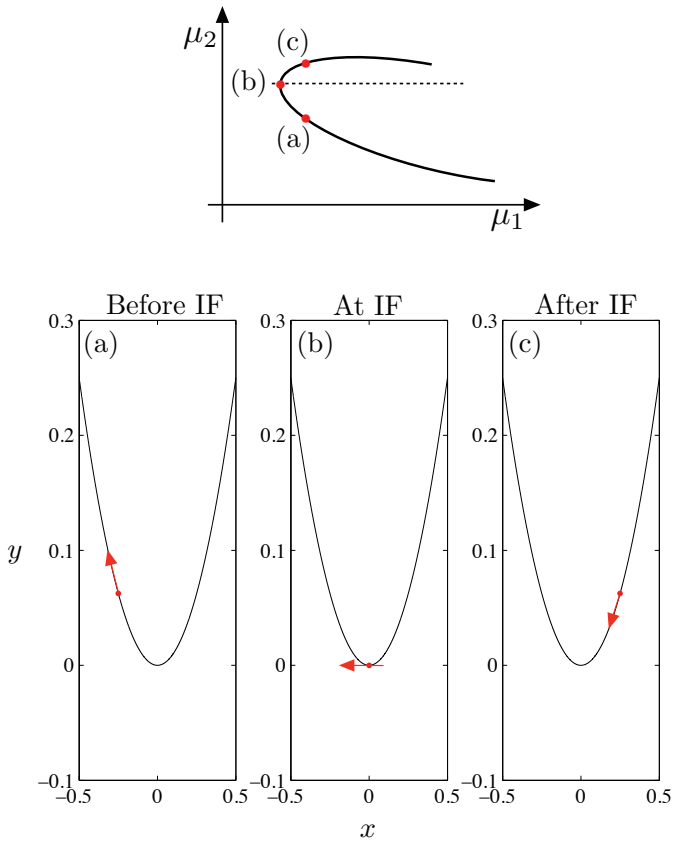

Figure 12. *Schematic representation of the return map computed for this system.*

the component of the one-dimensional stable manifold $W^s(p)$ that corresponds to $\gamma(0)$ when $\mu = 0$ is precisely given by $(\eta_1, \eta_2) = (\mu_1, \mu_2)$. See Figure 12.

We are now in a position to define leading-order Poincaré maps obtained by following trajectories between each of these Poincaré sections. The local map from $\Pi_0 : \Sigma_0 \to \Sigma_1$ can be obtained by solving the linear equations in a neighborhood of p. It is most useful in what follows to instead deal with $\Pi_0^{-1} : \Sigma_1 \to \Sigma_0$. Specifically, to leading order we obtain

$$\Pi_0^{-1} : \begin{pmatrix} \xi_1 \\ \varepsilon \\ \xi_3 \end{pmatrix} \mapsto \begin{pmatrix} \varepsilon \\ \xi_2 \\ \xi_3 \end{pmatrix} = \begin{pmatrix} \varepsilon \\ K_1 \xi_1^{\Delta_1} \\ K_2 \xi_3 \xi_1^{\Delta_2} \end{pmatrix},$$

where

$$0 < \Delta_2 = \frac{-\lambda_{uu}}{\lambda_s} < \Delta_1 = \frac{-\lambda_u}{\lambda_s}, \quad K_1 = \varepsilon^{1-\Delta_1}, \quad \text{and } K_2 = \varepsilon^{-\Delta_2}.$$

Hypothesis (H3) can now be encapsulated in the leading-order expression for the Poincaré map $\Pi_1 : \Sigma_1 \to \Sigma_2$. We construct this map in two stages. First consider the image of $W^u(p)$,

$$\begin{pmatrix} \eta_1 \\ \eta_2 \end{pmatrix} = \begin{pmatrix} \xi_3 \\ \beta \xi_3^2 \end{pmatrix},$$

where the unit coefficient of the η_1-term is chosen without loss of generality. Also, the η_2 coordinate is chosen so that $\beta > 0$. Moreover, the assumption (H3) of a sharp fold in the image of $W^u(p)$ implies

$$\beta\varepsilon \gg 1. \tag{3.1}$$

Thus the leading-order expression for the unit tangent vector to $W^u(p) \cap \Sigma$ is

$$\tau(\xi_3) = \begin{pmatrix} D(\xi_3) \\ 2\beta\xi_3 D(\xi_3) \end{pmatrix}, \quad \text{where} \quad D(\xi) = \frac{1}{\sqrt{1 + 4\beta^2\xi^2}}, \tag{3.2}$$

from which we obtain that the unit normal (in the sense of positive ξ_1 coordinate) is

$$\tau^{\perp}(\xi_3) = \begin{pmatrix} -2\beta\xi_3 D(\xi_3) \\ D(\xi_3) \end{pmatrix}.$$

Hence, the leading-order expression for the full map Π_1 can be written as

$$\Pi_1 : \begin{pmatrix} \xi_1 \\ \varepsilon \\ \xi_3 \end{pmatrix} \mapsto \begin{pmatrix} \eta_1 \\ \eta_2 \end{pmatrix} = \begin{pmatrix} \xi_3 - 2\beta\xi_1\xi_3 D(\xi_3) \\ \beta\xi_3^2 + \xi_1 D(\xi_3) \end{pmatrix}.$$

Finally, we suppose that the mapping $\Pi_2 : \Sigma_2 \to \Sigma_0$ is a diffeomorphism that can be expressed to leading order by its linear terms,

$$\Pi_2 : \begin{pmatrix} \eta_1 \\ \eta_2 \end{pmatrix} \mapsto \begin{pmatrix} \xi_2 \\ \xi_3 \end{pmatrix} = B \begin{pmatrix} \eta_1 - \mu_1 \\ \eta_2 - \mu_2 \end{pmatrix},$$

where $B = \{b_{ij}\}_{i,j=1,2}$ can be assumed generically to be an invertible matrix with all elements nonzero.

3.3. The inclination-flip bifurcation. In the context of the example system in question, an inclination flip is a codimension-two bifurcation that occurs when a path of homoclinic orbits to p undergoes a change in orientation.

From the construction above, the locus of homoclinic orbits to p in the μ-plane is given to leading order by

$$\mu_2 = \beta\mu_1^2, \tag{3.3}$$

which describes a sharp folded curve pointing along the positive μ_2-axis. For parameter values within this curve, the twistedness of the unstable manifold along the homoclinic loop γ can be computed by following the tangent vector to the stable manifold around the homoclinic orbit $\gamma(t)$.

Let (μ_1, μ_2) be a point within the homoclinic locus given by (3.3), and consider such a tangent vector with initial condition in the positive v_{uu} direction within Σ_1. By construction, the image of this initial condition under Π_1 is the vector $\tau(\mu_1)$ defined above (Figure 8). The image of $\tau(\mu_1)$ under Π_2 is then

$$\hat{\tau}(\mu_1) := \begin{pmatrix} (b_{11} + 2\beta b_{12}\mu_1)D(\mu_1) \\ (b_{21} + 2\beta b_{22}\mu_1)D(\mu_1) \end{pmatrix}.$$

Consider $\hat{\tau}$ for $\mu_1 = \varepsilon$. To leading order we find

$$\hat{\tau}(\varepsilon) = \begin{pmatrix} b_{12} \\ b_{22} \end{pmatrix},$$

in which we have used the form of D defined above (3.2) and the scaling (3.1). Now, under the nondegeneracy hypothesis that $b_{22} \neq 0$, as $t \to \infty$, the tangent vector will tend to $\mathrm{sign}(b_{22})\mathrm{v}_{uu}$.

A similar argument shows that the $\hat{\tau}$ in Σ_0 for $\mu_1 = -\varepsilon$ along the homoclinic locus maps is given by

$$\hat{\tau}(\varepsilon) = \begin{pmatrix} -b_{12} \\ -b_{22} \end{pmatrix}.$$

In turn, this vector tends to $-\mathrm{sign}(b_{22})\mathrm{v}_{uu}$ as $t \to \infty$.

Hence we have shown that the tangent vector to the homoclinic orbit, which is in the positive v_{uu} component as $t \to -\infty$, flips its v_{uu} component as $t \to +\infty$, for μ varying along the homoclinic locus (3.3) between $\mu_1 = \varepsilon$ and $\mu_1 = -\varepsilon$. This shows that there must be (at least one) inclination flip somewhere in between. In other words, there must be an orbit flip close to the sharp fold in the homoclinic locus.

3.4. Unfolding the dynamics near the inclination flip. It is straightforward to extend the analysis to provide a local asymptotic prediction of the bifurcations of periodic orbits that emanate from the inclination-flip point. Note that this is just one of a number of bifurcation curves that can be found to emanate from the inclination-flip point (see [33, 21]), but the point here is to produce an asymptotic formula that is valid in the present context of a folded manifold.

To this end we look for the simplest periodic orbits as fixed points of the return map

$$\Pi_2 \circ \Pi_1 \circ \Pi_0 : \Sigma_0 \to \Sigma_0.$$

In fact, it is most convenient to consider the Poincaré section Σ_2 and seek a condition for a fixed point in the form

$$\Pi_2^{-1} \circ \Pi_0^{-1}(\xi_1, \xi_3)^T = \Pi_1(\xi_1, \xi_3)^T.$$

To this end we find

$$\begin{pmatrix} \mu_1 \\ \mu_2 \end{pmatrix} + \hat{B} \begin{pmatrix} K_1 \xi_1^{\Delta_1} \\ K_2 \xi_3 \xi_1^{\Delta_2} \end{pmatrix} = \begin{pmatrix} \xi_3(1 - 2\beta\xi_1 D(\xi_3)) \\ \beta\xi_3^2 + \xi_1 D(\xi_3) \end{pmatrix},$$

where

$$\hat{B} = B^{-1} = \frac{1}{\det(B)} \begin{pmatrix} b_{22} & -b_{12} \\ -b_{21} & b_{11} \end{pmatrix}.$$

We now need to analyze these fixed point equations and find fold and flip bifurcations. We suppose we can do a rescaling so that $B = \mathrm{Id}$. Then the equations for the fixed points of the return map read

$$\begin{aligned} \mu_1 + K_1 \xi_1^{\Delta_1} &= \xi_3 - 2\beta\xi_1\xi_3 D(\xi_3), \\ \mu_2 + K_2 \xi_3 \xi_1^{\Delta_2} &= \beta\xi_3^2 + \xi_1 D(\xi_3). \end{aligned}$$

Given that β is assumed to be large ($\beta\varepsilon \gg 1$), we make the following approximation for ξ_3 such that it is at least of order 1, that is, "nonsmall":

$$D(\xi_3) := \frac{1}{\sqrt{1 + 4\beta^2\xi_3^2}} \approx \frac{1}{2\beta|\xi_3|}. \tag{3.4}$$

The fixed point equations (multiplying the second one by ξ_3) then reduce to

$$\begin{aligned} \mu_1 + K_1 \xi_1^{\Delta_1} &= \xi_3 \mp \xi_1, \\ \mu_2\xi_3 + K_2 \xi_1^{\Delta_2} \xi_3^2 &= \beta\xi_3^3 \pm \frac{\xi_1}{2\beta}. \end{aligned}$$

We look for μ_1- and μ_2-families of fixed points of the previous set of equations with AUTO [14]. We fix the signs and continue in μ_1 and in μ_2 the solutions to the system

$$\begin{aligned} \mu_1 + K_1 \xi_1^{\Delta_1} &= \xi_3 - \xi_1, \\ \mu_2\xi_3 + K_2 \xi_1^{\Delta_2} \xi_3^2 &= \beta\xi_3^3 + \frac{\xi_1}{2\beta}. \end{aligned}$$

These equations define saddle-node bifurcations of the fixed point which we can continue in two parameters to obtain a curve of fold points of the corresponding periodic orbits in the (μ_1, μ_2)-plane. In order to compute the curve of homoclinic bifurcations in this plane, we use the fact that, in the map Π_2, the homoclinic connection corresponds to

$$\eta_1 = \mu_1, \ \eta_2 = \mu_2.$$

In the preceding system of equations, this gives

$$K_1 \xi_1^{\Delta_1} = 0, \ K_2 \xi_1^{\Delta_2} \xi_3 = 0.$$

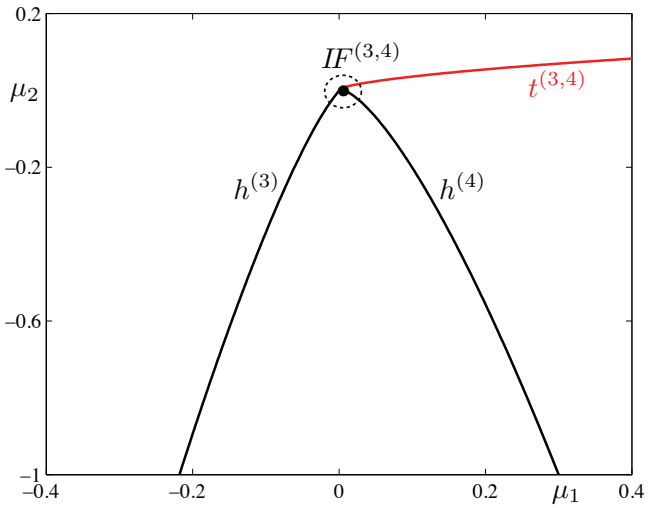

Figure 13. *Curve of fold and homoclinic bifurcation points in the (μ_1, μ_2)-plane, obtained from the return map that we derived above.*

Hence, we obtain the equation for the homoclinic curve

$$\mu_1 = \xi_3 - \xi_1,$$
$$\mu_2 = \beta\xi_3^2 + \frac{\xi_1}{2\beta\xi_3}.$$

We can then compare the computed curve of folds with the curve of homoclinic points, and we present the result in Figure 13. We obtain a qualitative agreement with the similar curves computed from the HR system. Indeed, the homoclinic curve is folded and, from the tip of that curve, corresponding to the inclination-flip bifurcation $IF^{(3,4)}$, emanates a curve of fold bifurcation, which corresponds to $t^{(3,4)}$. Note that our numerics are not valid in the vicinity of this tip (dashed circle in Figure 13); however, the trend of both the homoclinic and the fold curves outside this small region seems to indicate that they indeed meet at the tip.

For values of I and b corresponding to the numerical return map described above and to the inclination-flip bifurcation, we can compute the eigenvalue ratios $\Delta_2 = -\lambda_{uu}/\lambda_s$ and $\Delta_1 = -\lambda_u/\lambda_s$ and check where the point (Δ_2, Δ_1) is located in the diagram of Figure 4 (left) in [21], where different unfoldings of the inclination-flip bifurcation are studied. It appears that the HR system for the parameter values mentioned above falls into case C of the classification derived in [21]; therefore, horseshoe dynamics is expected in the vicinity of the inclination-flip point, which is consistent with the results of [40].

4. Discussion. This paper has revisited the well-known HR neuron model from a global bifurcation analysis standpoint. To this end, we used different tools, geometrical and numerical. We extracted specific information by relying on the strengths of each method and depicted a global bifurcation scenario by exploiting the tools' redundancy to overcome specific weaknesses of each method.

In particular, the analysis we have carried out has shown that numerical continuation based on boundary-value problems can be extremely useful in slow-fast systems where pure simulation can run into difficulties in unfolding bifurcations that are very close to one another. Note also that the homoclinic bifurcations studied here do not themselves represent stable dynamical behavior. Nevertheless, their influence on the global bifurcation structure is profound.

On the other hand, the geometrical analysis provided details that were not possible to obtain numerically. Moreover, the geometrical analysis points to a generic phenomenon. Namely, a sharp fold in the curve of homoclinic orbits in the parameter plane should usually (Figure 7 is an evident exception) be associated with an inclination flip. Such a phenomenon, for example, was also observed as part of the unfolding of a tangent period-to-equilibrium heteroclinic cycle [5].

The obtained bifurcation scenario is organized by various curves of homoclinic bifurcations and their codimension-two degeneracies and explains the smooth spike adding transition (where the number of spikes in each burst is increased by one) typical of the HR model and of many other neuron models. In some sense, the work presented here extends the work of Shilnikov and Kolomiets [35], who also detected the presence of inclination-flip and orbit-flip bifurcations in the HR neuron model. They found a wealth of complex dynamics; however, their bifurcation analysis was limited to the curve $h^{(1)}$, and the connection between codimension-two homoclinic bifurcations and period adding (the precise focus of our paper) is not treated. The results here have shown that the key to understanding the origins of the spike adding behavior is to analyze the inclination-flip and orbit-flip bifurcations occurring on the homoclinic curves $h^{(n)}$ for $n > 1$.

In [5], the analysis applies to the unfolding of a certain codimension-two heteroclinic tangency and is not specifically relevant to the present model. There, an inclination flip is argued to be the only possible codimension-two homoclinic bifurcation that explains a side-switching along certain curves of n-homoclinic bifurcations present in the unfolding. The present paper, therefore, adds further information to that analysis by showing the inclination flip to be a consequence of the sharp turning point of n-homoclinic bifurcation curves in that unfolding. It is also interesting to note that various sharp turning points of homoclinic curves in models of excitable systems are also discussed in [7]. However, in that case, the turning points were always close to a Hopf bifurcation of the underlying equilibrium and so not related to the case discussed here as the eigenvalues are always complex.

From a more practical point of view, all the stable time series one can obtain by integrating the HR neuron model (evidenced in the brute-force bifurcation diagrams) are organized by bifurcation curves, which are in turn organized by the codimension-two degeneracies illustrated in this paper, including the inclination-flip point not detected by HomCont, and analyzed by geometrical methods.

The analysis reported in this paper is interesting not only for its intrinsic value in explaining spike adding in the HR neuron model through codimension-two organizing points, but also because similar bifurcation structures have been found and analyzed in other studies. In particular, in [29] the authors perform a bifurcation analysis of a model of pancreatic β-cells, which show excitable features similar to those of neurons, and find a global bifurcation structure that strikingly resembles what we found for the HR model (see Figure 4 of the

cited paper). In [8, 34], the authors present an analysis of a reduced model of leech heart interneuron: also in this case, the period adding mechanism is regulated by the presence of homoclinic bifurcations and their degeneracies.

Obviously, a detailed bifurcation analysis of each model will show differences among models, but we dare say that the *global* bifurcation structure, i.e., the presence of homoclinic bifurcations and the interplay of period doubling and folds of cycle bifurcations, remains unchanged and constitutes a trademark of models of excitable cells that display the widespread period adding mechanism.

The analysis in this paper tells a coherent story. The new cascade of inclination flips we have found at turning points of n-homoclinic curves explains the folds of cycles that organize spike adding cascades. However, various *global aspects* of the bifurcation scenario remain to be investigated. For example, a further detailed unfolding in a neighborhood of the $IF(1)$ point seems to be required in order to understand the origin of each of the n-homoclinic loops. This would seem to require a new form of slow-fast analysis of a point in the parameter plane from which many curves seem to emanate and may well involve the canard-like growth of the 1-homoclinic orbit in the first place.

Finally, since the HR model is really a reduction of other more complex bursting models, it would also be interesting to see the extent to which the bifurcation structures described here are present in more physiologically based models that show spike adding behavior.

REFERENCES

[1] L. A. Belyakov, *A case of the generation of a periodic motion with homoclinic curves*, Mat. Zametki, 15 (1974), pp. 336–341.

[2] L. A. Belyakov, *The bifurcation set in a system with a homoclinic saddle curve*, Mat. Zametki, 28 (1980), pp. 910–916.

[3] L. A. Belyakov, *Bifurcation of systems with homoclinic curve of a saddle-focus with saddle quantity zero*, Math. Notes, 36 (1984), pp. 838–843.

[4] V. N. Belykh, I. V. Belykh, M. Colding-Jorgensen, and E. Mosekilde, *Homoclinic bifurcations leading to the emergence of bursting oscillations in cell models*, Eur. Phys. J. E, 3 (2000), pp. 205–219.

[5] A. R. Champneys, V. Kirk, E. Knobloch, B. E. Oldeman, and J. D. M. Rademacher, *Unfolding a tangent equilibrium-to-periodic heteroclinic cycle*, SIAM J. Appl. Dyn. Syst., 8 (2009), pp. 1261–1304.

[6] A. R. Champneys and Yu. A. Kuznetsov, *Numerical detection and continuation of codimension-2 homoclinic bifurcations*, Internat. J. Bifur. Chaos Appl. Sci. Engrg., 4 (1994), pp. 785–822.

[7] A. R. Champneys, V. Kirk, E. Knobloch, B. E. Oldeman, and J. Sneyd, *When Shil'nikov meets Hopf in excitable systems*, SIAM J. Appl. Dyn. Syst., 6 (2007), pp. 663–693.

[8] P. Channell, G. Cymbalyuk, and A. Shilnikov, *Origin of bursting through homoclinic spike adding in a neuron model*, Phys. Rev. Lett., 98 (2007), 134101.

[9] O. De Feo, G. M. Maggio, and M. P. Kennedy, *The Colpitts oscillator: Families of periodic solutions and their bifurcations*, Internat. J. Bifur. Chaos Appl. Sci. Engrg., 10 (2000), pp. 935–958.

[10] E. de Lange and M. Hasler, *Predicting single spikes and spike patterns with the Hindmarsh–Rose model*, Biol. Cybernet., 99 (2008), pp. 349–360.

[11] M. Desroches and M. R. Jeffrey, *Canards and curvature: The smallness of ε in slow-fast dynamics*, Proc. R. Soc. Lond. Ser. A Math. Phys. Eng. Sci., 467 (2011), pp. 2404–2421.

[12] M. Desroches, B. Krauskopf, and H. M. Osinga, *Numerical continuation of canard orbits in slow–fast dynamical systems*, Nonlinearity, 23 (2010), pp. 739–765.

[13] E. J. Doedel, B. Krauskopf, and H. M. Osinga, *Global bifurcations of the Lorenz manifold*, Nonlinearity, 19 (2006), pp. 2947–2972.

[14] E. J. Doedel and B. E. Oldeman, *AUTO-07P: Continuation and Bifurcation Software for Ordinary*

Differential Equations, Concordia University, Montreal, Quebec, Canada, 2009.
[15] N. Fenichel, *Geometric singular perturbation theory for ordinary differential equations*, J. Differential Equations, 31 (1979), pp. 53–98.
[16] J. M. González-Miranda, *Complex bifurcation structures in the Hindmarsh–Rose neuron model*, Internat. J. Bifur. Chaos Appl. Sci. Engrg., 17 (2007), pp. 3071–3083.
[17] J. Guckenheimer and C. Kuehn, *Computing slow manifolds of saddle type*, SIAM J. Appl. Dyn. Syst., 8 (2009), pp. 854–879.
[18] J. L. Hindmarsh and R. M. Rose, *A model of the nerve impulse using two first-order differential equations*, Nature, 296 (1982), pp. 162–164.
[19] J. L. Hindmarsh and R. M. Rose, *A model of neuronal bursting using three coupled first order differential equations*, Proc. Roy. Soc. London Ser. B Biol. Sci., 221 (1984), pp. 87–102.
[20] A. L. Hodgkin and A. F. Huxley, *A quantitative description of membrane current and its application to conduction and excitation in nerve*, J. Physiol. London, 117 (1952), pp. 500–544.
[21] A. J. Homburg and B. Krauskopf, *Resonant homoclinic flip bifurcations*, J. Dynam. Differential Equations, 12 (2000), pp. 807–850.
[22] A. J. Homburg and B. Sandstede, *Homoclinic and heteroclinic bifurcations in vector fields*, in Handbook of Dynamical Systems III, F. Takens, H. Broer, and B. Hasselblatt, eds., Elsevier, New York, 2010, pp. 379–524.
[23] G. Innocenti and R. Genesio, *On the dynamics of chaotic spiking-bursting transition in the Hindmarsh–Rose neuron*, Chaos, 19 (2009), 023124.
[24] E. M. Izhikevich, *Neural excitability, spiking and bursting*, Internat. J. Bifur. Chaos Appl. Sci. Engrg., 10 (2000), pp. 1171–1266.
[25] B. Krauskopf, H. M. Osinga, and J. Galán-Vioque, *Numerical Continuation Methods for Dynamical Systems. Path Following and Boundary Value Problems*, Springer-Verlag, New York, 2007.
[26] Y. A. Kuznetsov, *Elements of Applied Bifurcation Theory*, 3rd ed., Springer-Verlag, New York, 2004.
[27] Y. A. Kuznetsov, O. De Feo, and S. Rinaldi, *Belyakov homoclinic bifurcations in a tritrophic food chain model*, SIAM J. Appl. Math., 62 (2001), pp. 462–487.
[28] D. Linaro, *Nonlinear Dynamical Systems: Applications to Biological and Electronic Oscillators*, Ph.D. thesis, University of Genoa, Genoa, Italy, 2011.
[29] E. Mosekilde, B. Lading, S. Yanchuk, and Yu. Maistrenko, *Bifurcation structure of a model of bursting pancreatic cells*, BioSystems, 63 (2001), pp. 3–13.
[30] B. E. Oldeman, B. Krauskopf, and A. R. Champneys, *Death of period-doublings: Locating the homoclinic-doubling cascade*, Phys. D, 146 (2000), pp. 100–120.
[31] H. M. Osinga and K. T. Tsaneva-Atanasova, *Dynamics of plateau bursting depending on the location of its equilibrium*, J. Neuroendocrinology, 22 (2010), pp. 1301–1314.
[32] P. C. Rech, *Dynamics of a neuron model in different two-dimensional parameter-spaces*, Phys. Lett. A, 375 (2011), pp. 1461–1464.
[33] B. Sandstede, *Constructing dynamical systems having homoclinic bifurcation points of codimension two*, J. Dynam. Differential Equations, 9 (1997), pp. 269–288.
[34] A. Shilnikov, R. L. Calabrese, and G. Cymbalyuk, *Mechanism of bistability: Tonic spiking and bursting in a neuron model*, Phys. Rev. E, 71 (2005), 056214.
[35] A. Shilnikov and M. Kolomiets, *Methods of the qualitative theory for the Hindmarsh–Rose model: A case study. A tutorial*, Internat. J. Bifur. Chaos Appl. Sci. Engrg., 18 (2008), pp. 2141–2168.
[36] L. Shilnikov, *The existence of a denumerable set of periodic motions in four-dimensional space in an extended neighborhood of a saddle-focus*, Soviet Math. Dokl., 8 (1967), pp. 54–58.
[37] L. Shilnikov, *On the birth of a periodic motion from a trajectory bi-asymptotic to an equilibrium state of the saddle type*, Soviet Math. Sbornik, 35 (1968), pp. 240–264.
[38] L. Shilnikov and D. Turaev, *Methods of Qualitative Theory of Differential Equations and Related Topics*, Amer. Math. Soc. Transl. Ser. 2, AMS, Providence, RI, 2000.
[39] M. Storace, D. Linaro, and E. de Lange, *The Hindmarsh-Rose neuron model: Bifurcation analysis and piecewise-linear approximations*, Chaos, 18 (2008), 033128.
[40] D. Terman, *Chaotic spikes arising from a model of bursting in excitable membranes*, SIAM J. Appl. Math., 51 (1991), pp. 1418–1450.
[41] D. Terman, *The transition from bursting to continuous spiking in excitable membrane models*, J. Nonlinear Sci., 2 (1992), pp. 135–182.